ACS Photonics

Article

pubs.acs.org/journal/apchd5

Emission Engineering in Germanium Nanoresonators

Michele Celebrano,[†] Milena Baselli,[†] Monica Bollani,[‡] Jacopo Frigerio,[§] Andrea Bahgat Shehata,[∥] Adriano Della Frera,[∥] Alberto Tosi,[∥] Andrea Farina,[⊥] Fabio Pezzoli,[#] Johann Osmond,[△] Xiaofei Wu,[□] Bert Hecht,[□] Roman Sordan,[§] Daniel Chrastina,[§] Giovanni Isella,[§] Lamberto Duò,[†] Marco Finazzi,[†] and Paolo Biagioni*[,†]

[†]Dipartimento di Fisica and L-NESS, Politecnico di Milano, Piazza Leonardo da Vinci 32, 20133 Milano, Italy

[‡]Consiglio Nazionale delle Ricerche, Istituto di Fotonica e Nanotecnologie, Via Anzani 42, 22100 Como, Italy

[§]L-NESS, Dipartimento di Fisica, Politecnico di Milano, Polo Territoriale di Como, Via Anzani 42, 22100 Como, Italy

[∥]Dipartimento di Elettronica, Informazione e Bioingegneria, Politecnico di Milano, Piazza Leonardo da Vinci 32, 20133 Milano, Italy

[⊥]Consiglio Nazionale delle Ricerche, Istituto di Fotonica e Nanotecnologie, Piazza Leonardo da Vinci 32, 20133 Milano, Italy

[#]L-NESS, Dipartimento di Scienza dei Materiali, Università degli Studi di Milano-Bicocca, Via R. Cozzi 55, 20125 Milano, Italy

[△]ICFO-Institut de Ciéncies Fotoniques, Avenida Carl Friedrich Gauss, 3, 08860 Castelldefels, Barcelona, Spain

[□]Nano-Optics & Biophotonics Group, Department of Experimental Physics 5, Röntgen Research Center for Complex Materials (RCCM), Physics Institute, University of Würzburg, Am Hubland, 97074 Würzburg, Germany

Supporting Information

ABSTRACT: We experimentally investigate the smallest germanium waveguide cavity resonators on silicon that can be designed to work around 1.55 μm wavelength and observe an almost 30-fold enhancement in the collected spontaneous emission per unit volume when compared to a continuous germanium film of the same thickness. The enhancement is due to an effective combination of (i) excitation enhancement at the pump wavelength, (ii) emission enhancement (Purcell effect) at the emission wavelength, and (iii) effective beaming by the nanoresonators, which act as optical antennas to enhance the radiation efficiency. Our results set a basis for the understanding and engineering of light emission based on subwavelength, CMOS-compatible nanostructures operating at telecommunication wavelengths.

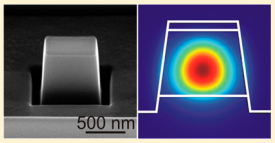

KEYWORDS: *silicon photonics, germanium emitter, optical antennas, waveguide resonators*

Over the past decade germanium has been proposed as one of the most promising materials for light detection, modulation, and emission in silicon-photonics architectures.[1−3] Its direct band gap, which is only about 140 meV larger than the fundamental indirect band gap,[4] ensures excellent absorption and promising emission properties, which recently led to the realization of integrated photodetectors[5−8] and electroluminescent devices[9,10] and to the demonstration of optically pumped[11] and electrically pumped[12] Ge lasers. An attractive feature of the Ge optical properties is the overlap between the direct emission band and the conventional telecommunication window around the 1.55 μm wavelength. Along the road toward integrated Ge light sources, significant efforts have been devoted to material engineering in terms of strain,[13−17] doping,[18,19] and dislocation management[20] in order to make radiative recombination more effective and create the conditions for population inversion and gain.[21,22] Also photonic engineering has been applied in order to establish cavity resonances at the desired emission wavelengths. Cavities based on photonic crystals have played a major role in this field, achieving large emission enhancement factors and high directionality.[23−25] A particularly appealing perspective, leading to compact and cost-effective solutions, is the direct shaping of the active Ge material as a cavity for photons, which allows one to spectrally purify, enhance, and redirect photon emission. While this concept has been successfully applied to the development of waveguide,[11,26] photonic-crystal,[27] and disk resonators,[28] the overall size of these photonic devices was generally much larger (from several μm to mm size) than the free-space operating wavelength λ_0, although, in principle, the volume of a resonant dielectric cavity can be as small as about $(\lambda_0/2n)^3$, n being the refractive index of the dielectric. It is one of the main paradigms of nano-optics that size reduction of modal volumes can increase light−matter interaction and boost light emission, also possibly reducing the threshold for lasing. Moreover, the trend toward smaller light sources is clearly driven by the perspective integration of nanodevices with largely reduced footprints.

In this work we design, fabricate, and experimentally characterize Ge nanoresonators on Si in the form of truncated waveguides with a fixed section profile of about 400 × 400 nm^2, i.e., very close to the cutoff conditions for the waveguide, and with a length L varying from 500 to 1400 nm. We characterize their cavity resonances by scanning confocal photoluminescence microscopy and observe on resonance a 27-fold

Received: June 13, 2014
Published: November 25, 2014

enhancement in the collected emission per unit volume when compared with a continuous Ge film having the same thickness.

The investigated nanostructures were fabricated by focused ion-beam (FIB) milling starting from a 400 nm thick Ge film heavily doped with phosphorus (activated dopant density $N_D \approx (1-2) \times 10^{19}$ cm^{-3}), grown on Si(001) wafers by low-energy plasma-enhanced chemical vapor deposition.[29] After the growth process, the sample was subjected to a series of annealing cycles between 600 and 780 °C to reduce the density of dislocations threading from the interface to the sample surface. Due to the difference between the thermal expansion coefficient of Ge and Si,[30,31] the Ge film acquires a tensile strain of approximately 0.22 ± 0.01%, as quantified by means of X-ray diffraction (see Supporting Information). The surface is then covered by a thermally evaporated silicon oxide film with a thickness of about 50 nm. Such a protective layer is extremely effective in improving the quality of FIB milling (see Supporting Information), and being transparent in the wavelength range considered here, it has no significant effects on the optical properties of the nanoresonators. The FIB patterning of the Ge epitaxial layers likely induces a modification of the thermally induced strain, since lateral dimensions become comparable with the film thickness. The original biaxial stress evolves toward a position-dependent triaxial stress,[32] and the formation of free surfaces is expected to allow, on average, elastic relaxation of the initial stress. A representative scanning electron microscopy (SEM) image of a resulting nanoresonator is shown in Figure 1a, where the protective SiO_x layer and the slightly tilted wall geometry are also visible.

The fabricated structures can be treated as finite pieces of waveguides, whose end facets act as cavity mirrors. Cavity resonances in such resonators originate from the self-interference of guided modes bouncing back and forth in the truncated waveguide while traveling along the y direction (see reference axis in Figure 1a). As a result, the local density of optical states available for the radiative decay of excited electron−hole pairs is suppressed off resonance and enhanced on resonance. In the latter case, the rate of spontaneous emission can therefore be increased, an effect known as the Purcell effect, which was originally invoked to describe lossless cavities but can be extended to lossy materials as well.[33] For a given guided mode with effective wavelength λ_{eff}, cavity resonances occur at waveguide lengths $L_{res} = m(\lambda_{eff}/2)$, where m is an integer defining the resonance order. We compute the spatial field distribution associated with each waveguide mode by means of the finite-difference frequency-domain (FDFD) method.[34] While for sections larger than about 400 × 400 nm^2 higher-order modes start to appear, for smaller sections cutoff conditions are gradually approached, with the guided modes being less and less confined inside the Ge waveguide (see Supporting Information). We find that, for a model waveguide made of the above-described material with a section of about 400 × 400 nm^2 in the xz plane and a free-space wavelength $\lambda_0 \cong 1550$ nm, only the two almost-degenerate lowest-order quasi-TE and quasi-TM modes are present (Figure 1b and c, respectively). Such modes are characterized by a dominant electric field oriented parallel and perpendicular to the substrate plane, respectively, and propagate in the y direction (see Figure 1b), along which cavity effects are established. The calculated index of these almost degenerate modes, for a geometry closely resembling the fabricated one, is $n \cong 3.6 + i0.01$, and their effective wavelength is therefore $\lambda_{eff} \cong 430$ nm.

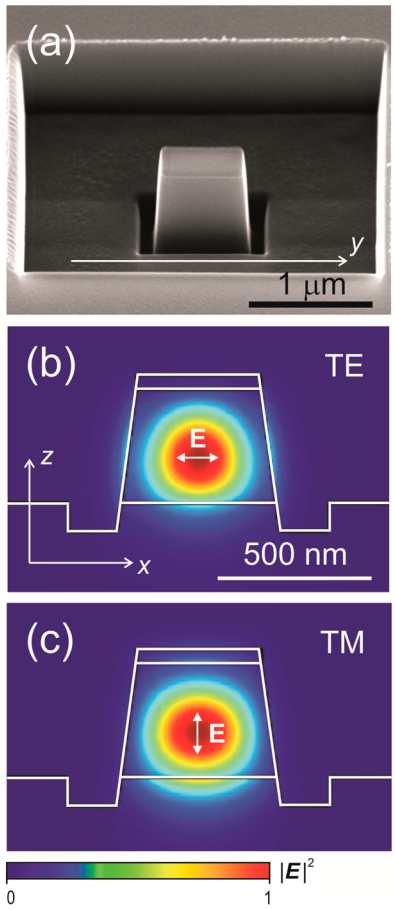

Figure 1. (a) SEM image of a Ge nanoresonator. The thin oxide protective layer and the slightly tilted lateral walls, due to the FIB beam profile, are also visible. Field intensity map of the lowest-order (b) quasi-TE and (c) quasi-TM mode in the Ge waveguide, calculated by FDFD on a model structure closely resembling the nanoresonators under study.

We recorded spatial maps collecting the direct-gap Ge spontaneous emission at room temperature by means of scanning confocal microscopy, employing a standard long-working-distance achromatic objective (N.A. = 0.7) and an excitation diode laser emitting at 980 nm wavelength, providing an experimental lateral resolution of about 1.3 μm (see Supporting Information). The average power impinging on the objective is kept in a range between 1 and 10 mW, corresponding to a power density of about 10^4−10^5 W/cm^2. The different spectral components of the collected emission are separated inside a Pellin-Broca prism[35] and then focused onto an InGaAs/InP single-photon avalanche diode (SPAD),[36] whose active area (25 μm diameter) acts as a spatial filter in the image plane for wavelength selection and background rejection. The spectral resolution is about 15 nm in the spectral range of interest.

Representative room-temperature luminescence maps of each individual nanoresonator, obtained by selecting a 15 nm spectral window around 1550 nm as determined by the resolution of the spectrometer, are shown in the bottom part of Figure 2, together with the respective SEM images. While for shorter resonators the confocal images show a single lobe as the result of the convolution between the nanostructure and the illumination Gaussian beam, cavities whose length is comparable with (or larger than) the lateral resolution of the

dx.doi.org/10.1021/ph500432k | ACS Photonics 2015, 2, 53−59

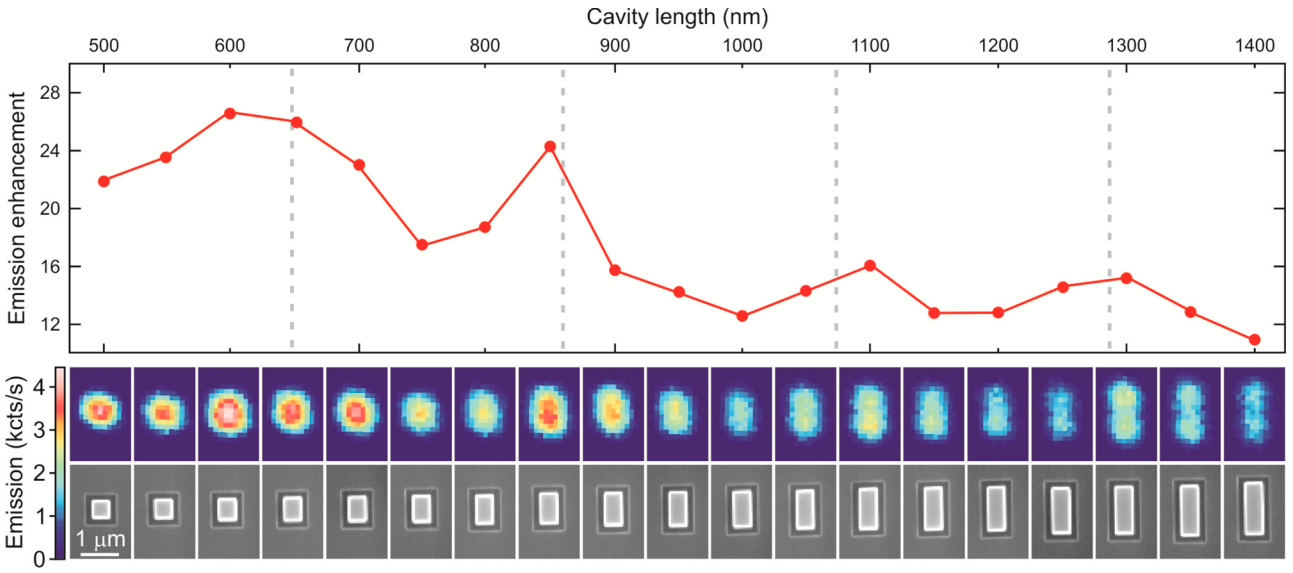

Figure 2. Lower panel: SEM and room-temperature confocal luminescence maps of the array of nanoresonators with length varying between about 500 and 1400 nm in steps of 50 nm. Upper panel: Experimental enhancement in the collected emission per unit volume from each individual Ge nanoresonator, normalized to the emission from a continuous Ge film of the same thickness. Each data point is the result of averaging over three different samples fabricated from the same Ge substrate with the same nominal dimensions. Dashed vertical lines represent the spectral position of cavity resonances expected on the basis of FDFD and FDTD simulations.

microscope show a double-lobe image. This can be interpreted, as already done in ref 26, as the result of waveguide-coupled emission being scattered by the poorly reflecting end-facet mirrors. A quantitative analysis of the measured enhancement is performed by extracting the emission per unit volume from the experimental map of each nanocavity and normalizing it to that of a continuous Ge film with the same thickness (unprocessed region of the same sample), taking the dimensions of the focal spot and the size of each nanostructure into account (see Supporting Information). The results are shown in the top part of Figure 2 as a function of the nanoresonator length, demonstrating an up to 27-fold enhancement in the collected emission intensity from the resonators compared to the film. A striking feature is the presence of maxima in the experimental emission enhancement for lengths roughly around 600, 850, 1100, and 1300 nm, i.e., with a length periodicity of about 235 nm. This value is in close coincidence with the periodicity of $(\lambda_{eff}/2) \cong 215$ nm expected for waveguide cavity resonances, as estimated from the FDFD simulations discussed above.

We performed a three-step analysis of the investigated sample geometry using FDTD simulations[37] in order to disentangle the different contributions to the observed overall enhancement (Figure 3a; see Supporting Information for details on the simulations). This approach considers (i) the enhancement in the absorbed power per unit volume by the resonator after 980 nm Gaussian beam illumination (red solid line, circles); (ii) the enhancement in the total emitted power at 1550 nm by a set of uncorrelated dipoles uniformly distributed inside the resonator to mimic spontaneous emission (blue line, triangles), and (iii) the enhancement due to changes in the emission directionality and radiation efficiency related to the fraction of emitted power falling within the objective's collection angle in the air half-space (black line, squares). Regarding the first contribution, it should be noted that no resonances are observed, as expected because of the large losses in the material at the pump wavelength. However, confined structures can nonresonantly absorb a larger fraction of power per unit volume than continuous films, for a fixed excitation fluency, because of the light-trapping contribution coming from high-index-contrast boundary conditions. The second contribution is calculated as the ratio of total emitted power by the dipoles inside the resonator and inside the continuous film. It should be noted that, in order to simulate uncorrelated dipoles and avoid spurious interference effects, N individual simulations need to be run to consider a set of N dipoles, one for each dipole. The third contribution is computed by projecting the local dipole fields to the far field and calculating the flux of the Poynting vector within the objective's collection angle. By combining the results of the three analysis steps, we are able to quantify the overall enhancement in the collected emission, as shown in Figure 3b (black line, circles). This is in excellent quantitative agreement with the experimental results (also shown in the same panel for comparison, red line, squares). The residual deviation between experimental and simulation results for the shorter nanoresonators may be due to a larger degree of elastic strain relaxation (and therefore lower efficiency for radiative recombination) as the length of the resonator is reduced,[38] or to the possible effect of surface defects created by the Ga ions during milling, which might play a role for shorter resonators. Overall, however, the very good agreement between simulations and experiments rules out a significant influence of FIB-induced defectivity, also thanks to the already discussed SiO_x protective layer.

Noticeably, most of the enhancement is related to the third contribution, i.e., to the enhanced radiation of the light emitted by the nanoresonators within the objective collection angle (antenna effect).[39] To gain a better understanding of the phenomenon, we plot in Figure 4 the emission angular pattern in the upper air half-space and in the lower Si half-space for a resonant structure (a) and for the continuous film (b). The same set of uncorrelated dipoles mentioned above is also used for these calculations. It can be seen that two effects take place in the nanoresonators compared to the continuous film: (i) an increase in the fraction of emitted photons that are beamed

dx.doi.org/10.1021/ph500432k | ACS Photonics 2015, 2, 53−59

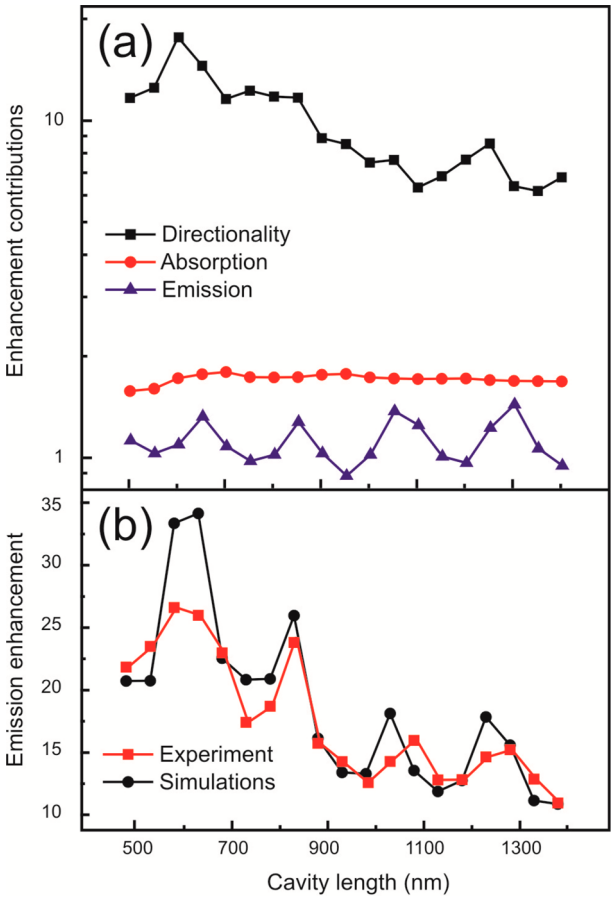

Figure 3. (a) Individual contributions to the total enhancement obtained from simulation results: increase in the absorbed power per unit volume (red line, circles), emission enhancement (blue line, triangles), and directional emission (black line, squares). (b) Results of FDTD simulations for the total enhancement per unit volume (black line, circles) and their quantitative comparison with the experimental results (red line, squares).

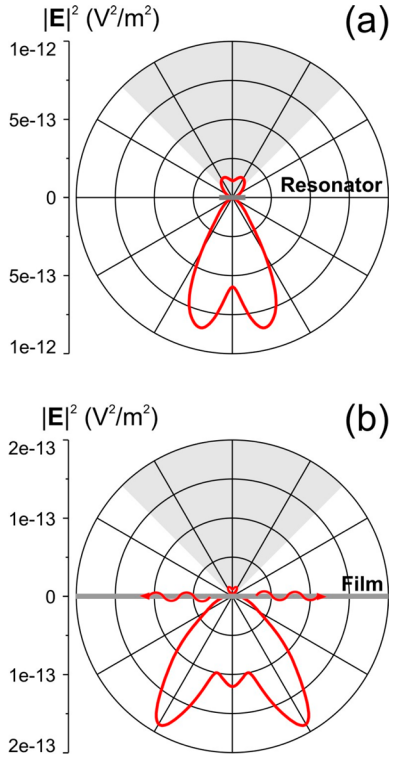

Figure 4. Angular distribution of the electric field intensity after far-field projection onto a sphere of 1 m radius, both for the upper air half-space and the lower Si half-space, for a set of uncorrelated dipoles emitting a total power of 1 W in a vacuum: (a) nanoresonator (L = 600 nm); (b) continuous Ge film of the same thickness. The angular patterns are plotted on a plane perpendicular to the resonator main axis. The gray cone represents the collection angle of the objective in the air half-space, while the wavy arrows represent nonradiative losses related to waveguided light trapping inside the Ge film. Note the different intensity scales for the two panels.

toward the air half-space compared with those that are emitted toward the substrate, with the nanoresonator beaming a larger fraction of the radiated photons toward the air half-space, and (ii) a drastic difference in the total number of radiated photons (note the different intensity scales for the two plots). The analysis shows that this drastic enhancement in the radiation efficiency is not related to a larger emission rate for the dipoles in the nanoresonator compared with the film; rather it is due to the large fraction of light that is waveguided and trapped inside the continuous film, which adds a further nonradiative loss channel for the film. The enhancement in the total emitted power (second step of the simulation analysis described above) is indeed particularly low due to the small quality factor of the resonances, mainly caused by the low reflectivity of the waveguide facets that is estimated to be around 68% (see Supporting Information). Nevertheless, contributions from waveguide cavity resonances are unambiguously detected as periodic oscillations in the emission signal as a function of the cavity length. In perspective, the quality factor of the resonances could be improved by fabricating steeper end facets or by a more advanced level of nanophotonic engineering, which would include for example nanostructured Bragg mirrors. It should also be noted that Figure 4 suggests that radiation enhancement into the substrate, although less substantial than the one toward the air half-space, is still significant and is also accompanied by an even more favorable beaming that reduces the angular width of the emitted photons and increases directionality.

Waveguide cavity resonances are also expected to have an effect on the spectral shape of the emission band, by enhancing those wavelength components that are on resonance with the cavity and suppressing those that are off resonance. Indeed, Figure 5a shows the periodic modulation of the emission spectrum measured on resonators of varying length and therefore varying resonant wavelength. The steep drop around 1600 nm represents the cutoff of the InGaAs/InP SPAD (see Supporting Information) and does not allow for a full quantitative analysis of the resulting spectral shape.

It should be noted that we observed no experimental dependence of the emitted intensity on the linear polarization direction of the excitation beam. This is due to the incoherent processes at the basis of spontaneous emission (where no memory is kept of the excitation polarization), which implies that the probability for an excited electron−hole pair to decay into a mode of the cavity with specific polarization properties is independent of the polarization of the excitation beam. Also, we found no net polarization of the emitted photons, meaning that the ratio $R = (I_{\perp}/I_{\parallel})$ between the emitted light intensity polarized perpendicular and parallel to the resonator axis is always around 1, with deviations below 30% among different

dx.doi.org/10.1021/ph500432k | ACS Photonics 2015, 2, 53−59

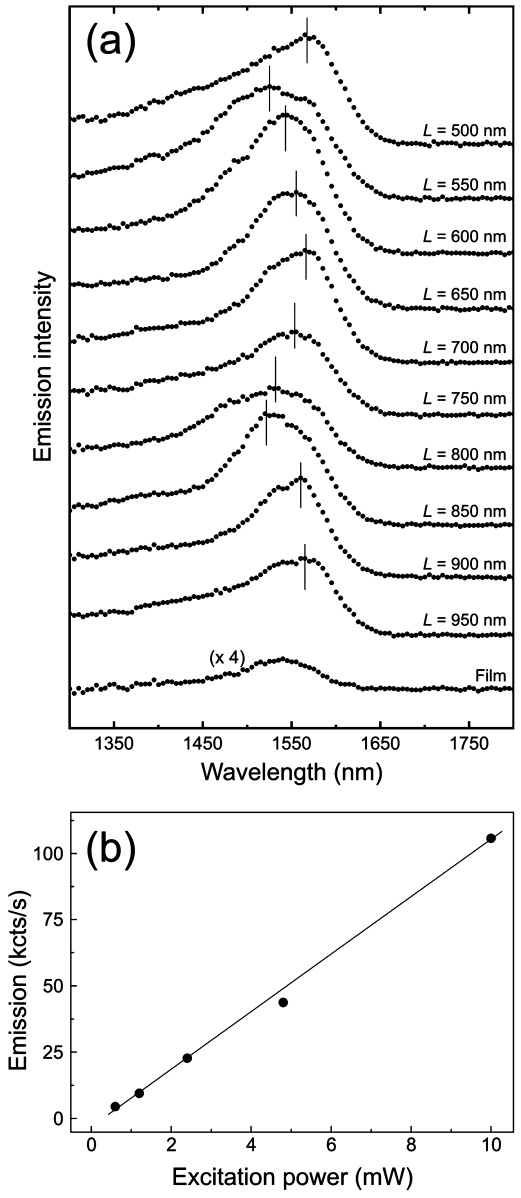

Figure 5. (a) Experimental room-temperature photoluminescence spectra from individual Ge nanoresonators and from the reference continuous Ge film, acquired with the same excitation power. (b) Representative emission rate from a resonant cavity as a function of the excitation power.

samples. While this would not be expected for an emission process mediated by a cavity, it should be recalled that the two almost degenerate quasi-TE and quasi-TM modes possess very different polarization properties. When this is taken into account and the far-field polarization for the ensemble of uncorrelated emitters is simulated, we find that only a residual $R \cong 2.5$ would be expected on average (see Supporting Information). We tentatively attribute the additional depolarization to residual wall roughness, which depolarizes the photons emitted by the Ge nanocavities. Finally, we experimentally observed a proportionality between the excitation power and the emission rate from the nanoresonators, as shown in Figure 5b, therefore finding no evidence of background due to thermal blackbody emission[40] and also ruling out any stimulated emission for the investigated excitation rates.

In conclusion, we studied the smallest possible waveguide cavity resonators that can be realized with Ge on Si and demonstrated an almost 30-fold enhancement in the collected emission per unit volume at 1.55 μm wavelength, when compared to that from a continuous film with the same thickness. Detailed simulations reveal that most of the enhancement is due to effective beaming of the emitted photons within the objective collection angle, demonstrating that the nanostructures act as efficient directional antennas to improve the radiation efficiency and confirming the key importance of a thorough analysis of emission enhancement processes from confined nanostructures to unambiguously assess their physical origin. In perspective, the performance of the resonators may be improved by strain engineering to further enhance the emission efficiency or by nanophotonic engineering of the cavity mirrors (e.g., fabricating steeper facets and/or Bragg reflectors) to enhance the quality factor of the resonances. The analysis and experimental results presented in this work therefore pave the way toward optimized group IV nanoemitters where doping, strain, and photonic engineering can all be merged together as different complementary ingredients to achieve highly directional and efficient nanoscale light sources at telecommunication wavelengths. Along this road, a full quantitative understanding and control of the emission processes of wavelength-sized resonators is a mandatory step. Applications of on-chip integrated incoherent light sources would be found, for example, for compact and cost-effective sensors that could require either air-coupled radiation (such as in photointerrupters, reflective photosensors, or any other sensor design that presents an air gap between the source and the detector) or waveguide-coupled emission (for example for refractive index sensing exploiting propagation along functionalized waveguides). The latter possibility could in principle also benefit from the well-defined mode profiles of the TM_0 and TE_0 modes supported by the Ge nanoresonators.

■ ASSOCIATED CONTENT

Supporting Information

Supporting Information provides further details on the X-ray diffraction strain analysis of the Ge sample, the FDFD and FDTD simulations, the ellipsometric characterization and emission spectrum of the Ge sample, the FIB milling procedure, the experimental confocal setup, the mode mapping and end-facet reflectivity in Ge-on-Si waveguides, the simulated polarization properties of emitted light, and the data analysis procedure for the experimental emission enhancement. This material is available free of charge via the Internet at http://pubs.acs.org.

■ AUTHOR INFORMATION

Corresponding Author

*E-mail: paolo.biagioni@polimi.it.

Notes

The authors declare no competing financial interest.

■ ACKNOWLEDGMENTS

The authors would like to thank J. Prangsma for insightful discussions on emission enhancement in lossy media and M. Barget for technical assistance. Funding from Fondazione Cariplo under the project 'Nano antennas of germanium for advanced photonics (NANOGAP)' (project number 2010-0632), from the European Union's Seventh Framework

Programme under grant agreement n° 613055, and from Regione Lombardia through the grant 'Dote ricercatori' is gratefully acknowledged.

REFERENCES

(1) Soref, R. Silicon photonics: a review of recent literature. *Silicon* **2010**, *2*, 1−6.
(2) Liang, D.; Bowers, J. E. Recent progress in lasers on silicon. *Nat. Photonics* **2010**, *4*, 511−517.
(3) Boucaud, P.; El Kurdi, M.; Ghrib, A.; Prost, M.; de Kersauson, M.; Sauvage, S.; Aniel, F.; Checoury, X.; Beaudoin, G.; Largeau, L.; Sagnes, I.; Ndong, G.; Chaigneau, M.; Ossikovski, R. Recent advances in germanium emission. *Photon. Res.* **2013**, *1*, 102−109.
(4) Grzybowski, G.; Roucka, R.; Mathews, J.; Jiang, L.; Beeler, R. T.; Kouvetakis, J.; Menéndez, J. Direct versus indirect optical recombination in Ge films grown on Si substrates. *Phys. Rev. B* **2011**, *84*, 205307.
(5) Osmond, J.; Isella, G.; Chrastina, D.; Kaufmann, R.; Acciarri, M.; von Känel, H. Ultralow dark current Ge/Si(100) photodiodes with low thermal budget. *Appl. Phys. Lett.* **2009**, *94*, 201106.
(6) Cao, L.; Park, J.-S.; Fan, P.; Clemens, B.; Brongersma, M. L. Resonant germanium nanoantenna photodetectors. *Nano Lett.* **2010**, *10*, 1229−1233.
(7) Kaufmann, R.; Isella, G.; Sanchez-Amores, A.; Neukom, S.; Neels, A.; Neumann, L.; Brenzikofer, A.; Dommann, A.; Urban, C.; von Känel, H. Near infrared image sensor with integrated germanium photodiodes. *J. Appl. Phys.* **2011**, *110*, 023107.
(8) Vivien, L.; Polzer, A.; Marris-Morini, D.; Osmond, J.; Hartmann, J. M.; Crozat, P.; Cassan, E.; Kopp, Ch.; Zimmermann, H.; Fédéli, J. M. Zero-bias 40Gbit/s germanium waveguide photodetector on silicon. *Opt. Express* **2012**, *20*, 1096−1101.
(9) Sun, X.; Liu, J.; Kimerling, L. C.; Michel, J. Room-temperature direct bandgap electroluminescence from Ge-on-Si light-emitting diodes. *Opt. Lett.* **2009**, *34*, 1198−1200.
(10) de Kersauson, M.; Jakomin, R.; El Kurdi, M.; Beaudoin, G.; Zerounian, N.; Aniel, F.; Sauvage, S.; Sagnes, I.; Boucaud, P. Direct and indirect band gap room temperature electroluminescence of Ge diodes. *J. Appl. Phys.* **2010**, *108*, 023105.
(11) Liu, J.; Sun, X.; Camacho-Aguilera, R.; Kimerling, L. C.; Michel, J. Ge-on-Si laser operating at room temperature. *Opt. Lett.* **2010**, *35*, 679−681.
(12) Camacho-Aguilera, R. E.; Cai, Y.; Patel, N.; Bessette, J. T.; Romagnoli, M.; Kimerling, L. C.; Michel, J. An electrically pumped germanium laser. *Opt. Express* **2012**, *20*, 11316−11320.
(13) El Kurdi, M.; Bertin, H.; Martincic, E.; de Kersauson, M.; Fishman, G.; Sauvage, S.; Bosseboeuf, A.; Boucaud, P. Control of direct band gap emission of bulk germanium by mechanical tensile strain. *Appl. Phys. Lett.* **2010**, *96*, 041909.
(14) Huo, Y.; Lin, H.; Chen, R.; Makarova, M.; Rong, Y.; Li, M.; Kamins, Th. I.; Vuckovic, J.; Harris, J. S. Strong enhancement of direct transition photoluminescence with highly tensile-strained Ge grown by molecular beam epitaxy. *Appl. Phys. Lett.* **2011**, *98*, 011111.
(15) Sánchez-Pérez, J. R.; Boztug, C.; Chen, F.; Sudradjat, F. F.; Paskiewicz, D. M.; Jacobson, R. B.; Lagally, M. G.; Paiella, R. Direct-bandgap light-emitting germanium in tensilely strained nanomembranes. *Proc. Natl. Acad. Sci. U.S.A.* **2011**, *108*, 18893−18898.
(16) Jain, J. R.; Hryciw, A.; Baer, Th. M.; Miller, D. A. B.; Brongersma, M. L.; Howe, R. T. A micromachining-based technology for enhancing germanium light emission via tensile strain. *Nat. Photonics* **2012**, *6*, 398−405.
(17) Süess, M. J.; Geiger, R.; Minamisawa, R. A.; Schiefler, G.; Frigerio, J.; Chrastina, D.; Isella, G.; Spolenak, R.; Faist, J.; Sigg, H. Analysis of enhanced light emission from highly strained germanium microbridges. *Nat. Photonics* **2013**, *7*, 466−472.
(18) Liu, J.; Sun, X.; Pan, D.; Wang, X.; Kimerling, X. W.; Koch, Th. L.; Michel, J. Tensile-strained n-type Ge as a gain medium for monolithic laser integration on Si. *Opt. Express* **2007**, *15*, 11272−11277.
(19) El Kurdi, M.; Kociniewski, T.; Ngo, T.-P.; Boulmer, J.; Débarre, D.; Boucaud, P.; Damlencourt, J. F.; Kermarrec, O.; Bensahel, D. Enhanced photoluminescence of heavily n-doped germanium. *Appl. Phys. Lett.* **2009**, *94*, 191107.
(20) Pezzoli, F.; Isa, F.; Isella, G.; Falub, C. V.; Kreiliger, T.; Salvalaglio, M.; Bergamaschini, R.; Grilli, E.; Guzzi, M.; von Känel, H.; Miglio, L. Ge Crystals on Si show their light. *Phys. Rev. Applied* **2014**, *1*, 044005.
(21) Carroll, L.; Friedli, P.; Neuenschwander, S.; Sigg, H.; Cecchi, S.; Isa, F.; Chrastina, D.; Isella, G.; Fedoryshyn, Y.; Faist, J. Direct-gap gain and optical absorption in germanium correlated to the density of photoexcited carries, doping, and strain. *Phys. Rev. Lett.* **2012**, *109*, 057402.
(22) Dutt, B.; Sukhdeo, D. S.; Nam, D.; Vulovic, B. M.; Yuan, S.; Saraswat, K. C. Roadmap to an efficient germanium-on-silicon laser: strain vs. n-type doping. *IEEE Photonics J.* **2012**, *4*, 2002−2009.
(23) Portalupi, S. L.; Galli, M.; Reardon, C.; Krauss, T. F.; O'Faolain, L.; Andreani, L. C.; Gerace, D. Planar photonic crystal cavities with far-field optimization for high coupling efficiency and quality factor. *Opt Express* **2010**, *18*, 16064−16073.
(24) Römer, F.; Witzigmann, B. Spectral and spatial properties of the spontaneous emission enhancement in photonic crystal cavities. *J. Opt. Soc. Am. B* **2008**, *25*, 31−39.
(25) Toishi, M.; Englund, D.; Faraon, A.; Vučković, J. High-brightness single photon source from a quantum dot in a directional emission nanocavity. *Opt. Express* **2009**, *17*, 14618−14626.
(26) de Kersauson, M.; El Kurdi, M.; David, S.; Checoury, X.; Fishman, G.; Sauvage, S.; Jakomin, R.; Beaudoin, G.; Sagnes, I.; Boucaud, P. Optical gain in single tensile-strained germanium photonic wire. *Opt. Exp.* **2011**, *19*, 17925−17934.
(27) Boucaud, P.; El Kurdi, M.; David, S.; Checoury, X.; Li, X.; Ngo, T.-P.; Sauvage, S.; Bouchier, D.; Fishman, G.; Kermarrec, O.; Campidelli, Y.; Bensahel, D.; Akatsu, T.; Richtarch, C.; Ghyselen, B. Germanium-based nanophotonic devices: two-dimensional photonic crystals and cavities. *Thin Solid Films* **2008**, *517*, 121−124.
(28) Shambat, G.; Cheng, S.-L.; Lu, J.; Nishi, Y.; Vuckovic, J. Direct band Ge photoluminescence near 1.6 μm coupled to Ge-on-Si microdisk resonators. *Appl. Phys. Lett.* **2010**, *97*, 241102.
(29) Rosenblad, C.; Deller, H. R.; Dommann, A.; Meyer, T.; Schroeter, P.; von Känel, H. Silicon epitaxy by low-energy plasma enhanced chemical vapor deposition. *J. Vac. Sci. Technol. A* **1998**, *16*, 2785−2790.
(30) Slack, G. A.; Bartram, S. F. Thermal expansion of some diamondlike crystals. *J. Appl. Phys.* **1975**, *46*, 89−98.
(31) Capellini, G.; De Seta, M.; Zaumseil, P.; Kozlowski, G.; Schroeder, T. High temperature x ray diffraction measurements on Ge/Si(001) heterostructures: A study on the residual tensile strain. *J. Appl. Phys.* **2012**, *111*, 073518.
(32) Jain, S. C.; Harker, A. H.; Atkinson, A.; Pinardi, K. J. Edge-induced stress and strain in stripe films and substrates: A two-dimensional finite element calculation. *Appl. Phys.* **1995**, *78*, 1630−1637.
(33) Sauvan, C.; Hugonin, J. P.; Maksymov, I. S.; Lalanne, P. Theory of the spontaneous optical emission of nanosize photonic and plasmon resonators. *Phys. Rev. Lett.* **2013**, *110*, 237401.
(34) *MODE Solutions*, version 6.0.3; Lumerical Solutions, Inc.: Canada, 2013.
(35) Bargigia, I.; Tosi, A.; Bahgat Shehata, A.; Della Frera, A.; Farina, A.; Bassi, A.; Taroni, P.; Dalla Mora, A.; Zappa, F.; Cubeddu, R.; Pifferi, A. Time-resolved diffuse optical spectroscopy up to 1700 nm by means of a time-gated InGaAs/InP single-photon avalanche diode. *Appl. Spectrosc.* **2012**, *66*, 944−950.
(36) Tosi, A.; Della Frera, A.; Bahgat Shehata, A.; Scarcella, C. Fully programmable single-photon detection module for InGaAs/InP single-photon avalanche diodes with clean and sub-nanosecond gating transitions. *Rev. Sci. Instrum.* **2012**, *83*, 013104.
(37) *FDTD Solutions*, version 8.5.3; Lumerical Solutions, Inc.: Canada, 2013.

(38) Chrastina, D.; Vanacore, G. M.; Bollani, M.; Boye, P.; Schöder, S.; Burghammer, M.; Sordan, R.; Isella, G.; Zani, M.; Tagliaferri, A. Patterning-induced strain relief in single lithographic SiGe nanostructures studied by nanobeam x-ray diffraction. *Nanotechnology* **2012**, *23*, 155702.
(39) Biagioni, P.; Huang, J.-S.; Hecht, B. Nanoantennas for visible and infrared radiation. *Rep. Prog. Phys.* **2012**, *75*, 024402.
(40) Boucaud, P.; El Kurdi, M.; Sauvage, S.; de Kersauson, M.; Ghrib, A.; Checoury, X. Light emission from strained germanium. *Nat. Photonics* **2013**, *7*, 162.